CONTRAST MEDIA & MOLECULAR IMAGING

Received: 26 June 2012, Revised: 6 November 2012, Accepted: 11 December 2012, Published online in Wiley Online Library

(wileyonlinelibrary.com) DOI: 10.1002/cmmi.1526

Evaluation of the novel USPIO GEH121333 for MR imaging of cancer immune responses

Qiaoyun Shi[a], Laura J. Pisani[a], Yauk K. Lee[b], Solomon Messing[c], Celina Ansari[a], Srabani Bhaumik[d], Lisa Lowery[d], Brian D. Lee[d], Dan E. Meyer[d] and Heike E. Daldrup-Link[a]*

Tumor-associated macrophages (TAM) maintain a chronic inflammation in cancers, which is associated with tumor aggressiveness and poor prognosis. The purpose of this study was to: (1) evaluate the pharmacokinetics and tolerability of the novel ultrasmall superparamagnetic iron oxide nanoparticle (USPIO) compound GEH121333; (2) assess whether GEH121333 can serve as a MR imaging biomarker for TAM; and (3) compare tumor MR enhancement profiles between GEH121333 and ferumoxytol. Blood half-lives of GEH121333 and ferumoxytol were measured by relaxometry ($n = 4$ each). Tolerance was assessed in healthy rats injected with high dose GEH121333, vehicle or saline ($n = 4$ each). Animals were monitored for 7 days regarding body weight, complete blood counts and serum chemistry, followed by histological evaluation of visceral organs. MR imaging was performed on mice harboring MMTV-PyMT-derived breast adenocarcinomas using a 7 T scanner before and up to 72 h post-injection (p.i.) of GEH121333 ($n = 10$) or ferumoxytol ($n = 9$). Tumor R_1, R_2* relaxation rates were compared between different experimental groups and time points, using a linear mixed effects model with a random effect for each animal. MR data were correlated with histopathology. GEH121333 showed a longer circulation half-life than ferumoxytol. Intravenous GEH121333 did not produce significant adverse effects in rats. All tumors demonstrated significant enhancement on T_1, T_2 and T_2*-weighted images at 1, 24, 48 and 72 h p.i. GEH121333 generated stronger tumor T_2* enhancement than ferumoxytol. Histological analysis verified intracellular compartmentalization of GEH121333 by TAM at 24, 48 and 72 h p.i. MR imaging with GEH121333 nanoparticles represents a novel biomarker for TAM assessment. This new USPIO MR contrast agent provides a longer blood half-life and better TAM enhancement compared with the iron supplement ferumoxytol. Copyright © 2013 John Wiley & Sons, Ltd.

Supporting information may be found in the online version of this paper

Keywords: iron oxide nanoparticles; USPIO; ferumoxytol; GEH121333; macrophage; MR imaging; tumor imaging

1. INTRODUCTION

Pre-clinical and clinical investigations have shown that pro-inflammatory leukocytes regulate the development and progression of a large variety of cancers, including lung, breast, colon, prostate, cervical, liver, ovarian, lymphoma and thyroid cancers and some pediatric solid malignancies (1–4). Tumor-associated macrophages (TAM) play a key role in this process (5). They secrete growth factors that support the proliferation of neoplastic cells, along with delivering vascular endothelial growth factor (VEGF) to activate tumor angiogenesis (6,7) and produce cytokines and extracellular proteases to support tumor invasion and metastasis (1,2,4,8–11). The degree of TAM infiltration in malignant tumors is positively correlated with disease aggressiveness and worse clinical outcomes (4,12–14). New therapeutic drugs that target TAM are currently being developed and are starting to enter the clinic (15–17). Thus, it becomes increasingly important to identify patients whose tumors are heavily infiltrated by TAM, in order to stratify these patients to TAM-depleting therapies and to monitor response to these new therapies. To serve this goal, a noninvasive and easily repeatable imaging test would be advantageous over invasive biopsy. Ultrasmall superparamagnetic iron oxide nanoparticle (USPIO) can be used for selective visualization of TAM with magnetic resonance (MR) imaging (18,19). Upon intravenous injection, USPIOs slowly extravasate across the leaky tumor vasculature and accumulate in the tumor interstitium (EPR: enhanced permeability and retention), where they are phagocytosed by TAM (20). We previously reported that significant T_2-effects in tumors on delayed MR images, acquired at 24 h post-contrast, corresponded to USPIO uptake and retention by TAM as revealed by immunohistopathology (18,21). In addition, TAM depletion using specific

* *Correspondence to: H. E. Daldrup-Link, Department of Radiology, Molecular Imaging Program at Stanford, Stanford University, Stanford, CA 94305, USA. Email: heiked@stanford.edu*

a *Q. Shi, L. J. Pisani, C. Ansari, H. E. Daldrup-Link*
Department of Radiology, Molecular Imaging Program at Stanford, Stanford University, Stanford, CA, 94305, USA

b *Y. K. Lee*
Department of Radiology, Santa Clara Valley Medical Center, 751 South Bascom Avenue, San Jose, CA, 95128, USA

c *S. Messing*
Departments of Communication and Statistics, Stanford University, Stanford, CA, USA

d *S. Bhaumik, L. Lowery, B. D. Lee, D. E. Meyer*
Biomedical Imaging & Physiology Laboratory, GE Global Research Center, Niskayuna, NY, 12309, USA

monoclonal antibodies inhibited USPIO-induced tumor MR enhancement *in vivo* (18).

In order to translate experimental TAM imaging results to clinical practice, clinically applicable USPIO are needed. Ferumoxytol (Feraheme™) is a US Food and Drug Administration (FDA) approved iron supplement, which can be used 'off label' as a contrast agent for MR imaging (22–24). However, ferumoxytol has two disadvantages: first, an investigational new drug application is required to use ferumoxytol as a contrast agent, making it complicated in everyday practice. Second, ferumoxytol injection has been associated with an increased frequency of allergic reactions, most likely because of the carboxydextran coating of the drug (25). To overcome these limitations, GEH121333 has been developed as a novel, dedicated USPIO contrast agent for MR imaging. GEH121333 is composed of an Fe_3O_4 core and a hydroxyphosphonate–polyethylene glycol (PEG) shell (US patent 20110104072 A1). Based on the vast experience with PEG coatings in various drugs (26–28), GEH121333 nanoparticles are expected to initiate minimal adverse reactions after intravenous administration.

The purpose of this study was to (A) evaluate the pharmacokinetics and tolerability of the novel iron oxide nanoparticle compound GEH121333 in rodents, (B) assess if GEH121333 can serve as an MR imaging biomarker for TAM, and (C) compare tumor MR enhancement profiles between GEH121333 and ferumoxytol.

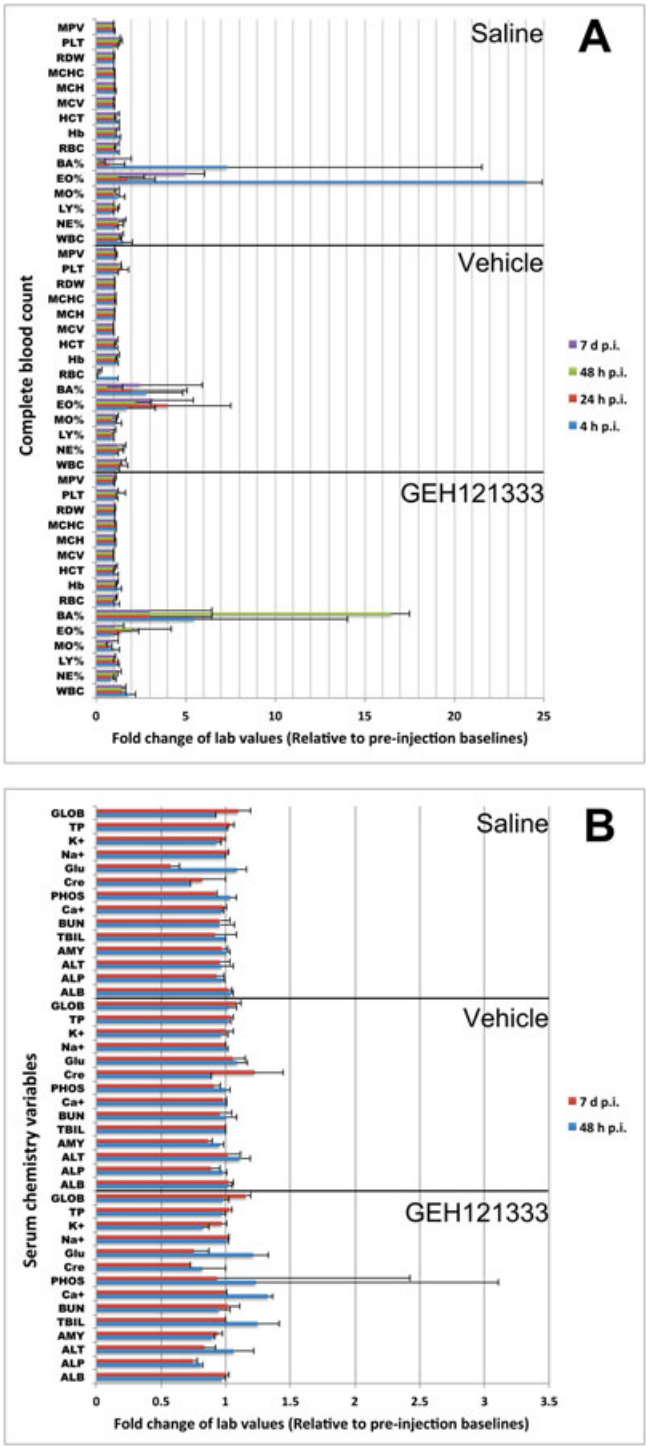

2. RESULTS

2.1. Pharmacokinetic and Tolerance Evaluation of GEH121333

An initial pharmacokinetic study assessed the blood half-life in rats by blood relaxometry. The relative standard error of the T_1 and T_2 measurements was ~5%. The blood half-life was estimated as 2.3 and 1.8 h (based on T_1 and T_2 data, respectively) for ferumoxytol, and as 3.8 and 4.0 h for GEH121333.

The high-dose tolerability study with GEH121333 (200 mg Fe kg^{-1}) did not reveal any weight loss in GEH121333-injected rats compared with controls. During daily weight measurement study, all animals showed a slight, nonsignificant weight gain over 7 days. Complete blood count (CBC, Fig. 1A) revealed that all animals presented a transient lymphocytosis at 4 h post-injection (p.i.), with significant, 60–80% increase in neutrophils and lymphocytes compared with pre-contrast data ($p < 0.05$). There was no significant difference between GEH121333-injected animals and controls ($p > 0.05$). Serum chemistry data (Fig. 1B) did not change significantly at 48 h and 7 days after injection of contrast agent or vehicle ($p > 0.05$). We were unable to evaluate serum chemistry panels at 4 and 24 h p.i. of GEH121333 owing to colorimetric interference resulting from the discoloration of the blood by USPIO. At 7 days post-injection, no significant gross pathological abnormalities were observed in any animals treated with GEH121333, vehicle or saline. Microscopic evaluations did not reveal significant structural abnormality of reticuloendothelial system (RES) organs (liver, spleen and bone marrow), heart, lungs and kidneys in any of the animals. There was moderate

Figure 1. No clinically significant changes in complete blood count and serum chemistry after high dose GEH121333 injection. Intravenous injection of GEH121333 at 200 mg Fe kg^{-1} did not generate clinically significant alteration in complete blood count (A) and serum chemistry (B) profiles up to 7 days p.i. compared with laboratory values of vehicle or saline-treated animals. MPV, mean platelet volume; PLT, platelet count; RDW, red blood cell distribution width; MCHC, mean corpuscular hemoglobin concentration; MCH, mean corpuscular hemoglobin; MCV, mean corpuscular volume; HCT, hematocrit; Hb, hemoglobin; RBC, red blood cell count; BA%, percentage basophil count; EO%, percentage eosinophil count; MO%, percentage monocyte count; LY%, percentage lymphocyte count; NE%, percentage neutrophil count; WBC, white blood cell count; GLOB, globulin; TP, total protein; K^+, potassium; Na^+, sodium; Glu, glucose; Cre, creatinine; PHOS, phosphate; Ca^+, calcium; BUN, blood urea nitrogen; TBIL, total bilirubin; AMY, amylase; ALT, alanine transaminase; ALP, alkaline phosphatase; ALB, albumin.

Kupffer cell pigmentation in rat livers after GEH121333 administration, probably owing to contrast agent-induced discoloration. No clinically significant liver pathology was found, supported by normal liver enzymes and serum chemistry data. We also discovered mild extramedullary hematopoiesis in rat spleens, which was not significantly different between GEH121333-injected and control animals. In summary, no significant adverse effects were observed in animals treated with GEH121333 at a high dose of 200 mg Fe kg^{-1}.

2.2. GEH121333 Produced Significant and Persistent Tumor Enhancement

GEH121333 nanoparticles induced a marked, inhomogeneous, and sustained tumor enhancement on T_1, T_2 and T_2*-weighted MR images (Fig. 2). GEH121333 significantly increased R_1 ($p = 0.0291$) and R_2* ($p < 0.0001$) relaxation rates at each post-contrast time point (Fig. 3). Tumor R_1 relaxation rates started to increase in the early post-contrast phase at 1 h, reached the maximum at 24–48 h p.i. followed by a gradual recovery that did not return to the pre-contrast baseline at 72 h p.i. Tumor T_2* enhancement occurred on early post-contrast scans at 1 h, further increased up to 24 h, and persisted at 48 and 72 h p.i. No significant recovery of tumor R_2* relaxation rates was found in the above post-contrast time frames. The decoupling between R_1 and R_2* relaxation rates at 72 h p.i. was attributed to clearance of extracellular GEH121333 (R_1) and persistent intracellular compartmentalization of nanoparticles in TAM (R_2*) (Fig. 5C). Histological analysis verified intracellular compartmentalization of GEH121333 by TAM.

2.3. Comparison Between GEH121333 and Ferumoxytol

Both GEH121333 and ferumoxytol induced T_1 enhancement in tumors (Fig. 3). Post-contrast R_1 relaxation rates and quantitative ΔR_1 data showed no significant differences ($p > 0.05$) between GEH121333-treated tumors (Supporting Information, mean $\Delta R_1 = 0.054$, 0.217, 0.094 and 0.044 at 1, 24, 48 and 72 h p.i., respectively) and ferumoxytol-treated tumors (mean $\Delta R_1 = 0.009$, 0.094, 0.043 and 0.022 at 1, 24, 48 and 72 h p.i., respectively).

As shown on R_2* relaxation rate maps (Fig. 4), tumors on pre-contrast scans showed relatively homogenous and low-baseline R_2* values. After GEH121333 and ferumoxytol administration, there was a generalized increase in tumor R_2*. GEH121333 generated a stronger T_2* effect than ferumoxytol ($p = 0.0066$). Quantitative ΔR_2* demonstrated a significantly stronger tumor enhancement in GEH121333-injected animals (Supporting Information, mean ΔR_2* = 252.1, 433.0, 363.0 and 345.5 at 1, 24, 48 and 72 h p.i., respectively) as compared with ferumoxytol-injected ones (mean ΔR_2* = 145.1, 133.8, 94.7, 70.3 at 1, 24, 48, 72 h p.i., respectively).

2.4. GEH121333-induced T_2 and T_2* Enhancement Corresponded to TAM-mediated Uptake

At 24, 48 and 72 h after injection of GEH121333 or ferumoxytol, Perls stain identified numerous blue-colored cells laced around the border of the tumor and in some focal areas within the tumor center, suggesting intracellular iron deposition (Fig. 5A, B). Blue-stained cell patches were often found around blood vessels. Some areas in untreated tumors also showed iron-positive cells, although far fewer than in USPIO-treated ones. Immunofluorescence assay confirmed TAM infiltration and USPIO deposition in GEH121333-injected tumors (Fig. 5C). Co-localization of GEH121333 coating (red) and TAM (green) indicated intracellular retention of GEH121333 in TAM (yellow/orange).

3. DISCUSSION

GEH121333 could be used as an imaging biomarker for TAM. This novel, dedicated MR contrast agent showed prolonged blood half-

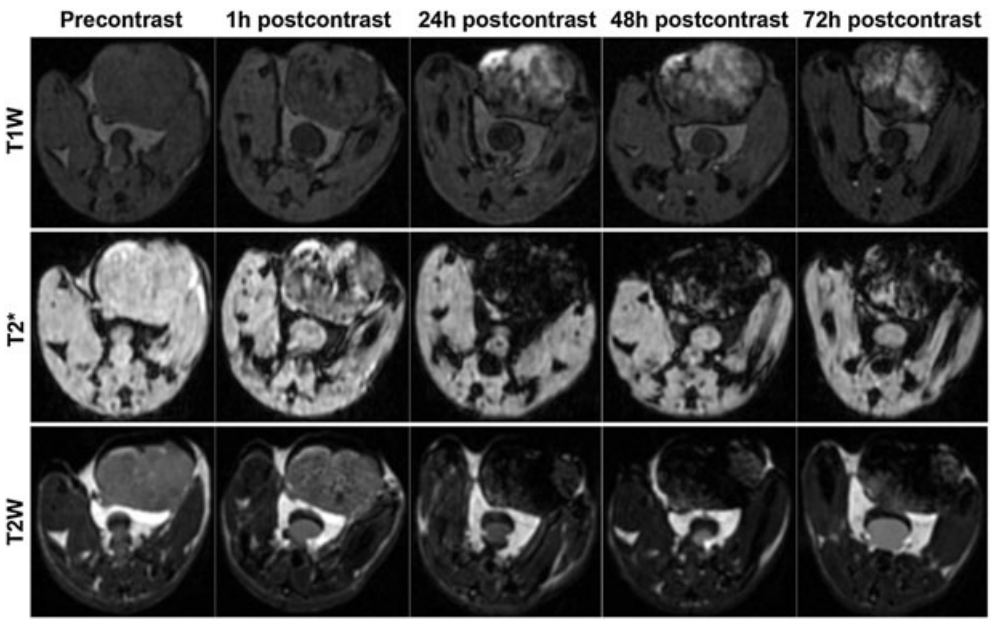

Figure 2. GEH121333-induced tumor T_1, T_2 and T_2* enhancement. Representative axial T_1, T_2 and T_2*-weighted images of mouse adenocarcinomas before and after GEH121333 injection. On early post-contrast images, GEH121333 caused mild T_1, T_2 and T_2* enhancement. Subsequent, delayed acquisitions at 24, 48 and 72 h post-contrast administration revealed marked, inhomogeneous, and persistent tumor signal enhancement on T_1 images, along with tumor signal loss on T_2 and T_2* images.

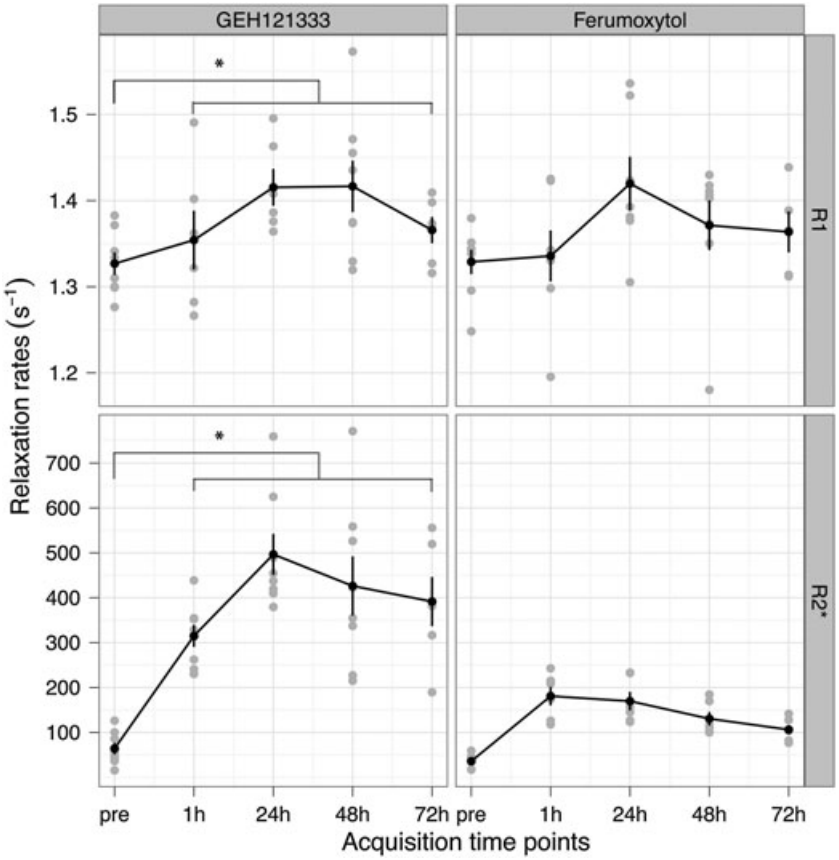

Figure 3. GEH121333 increased tumor R_1 and R_2* relaxation rates. Quantitative R_1 and R_2* relaxation rates of adenocarcinomas before (pre) and at different time points (1, 24, 48 and 72 h) after intravenous injection of GEH121333 and ferumoxytol are presented. GEH121333 caused a significant increase in R_1 and R_2* relaxation rates. Data are displayed as means and standard deviations acquired from 10 GEH121333-treated tumors and nine ferumoxytol-treated ones. The asterisk indicates statistical significance ($p < 0.05$) in post-contrast relaxation rates compared with the pre-contrast baseline.

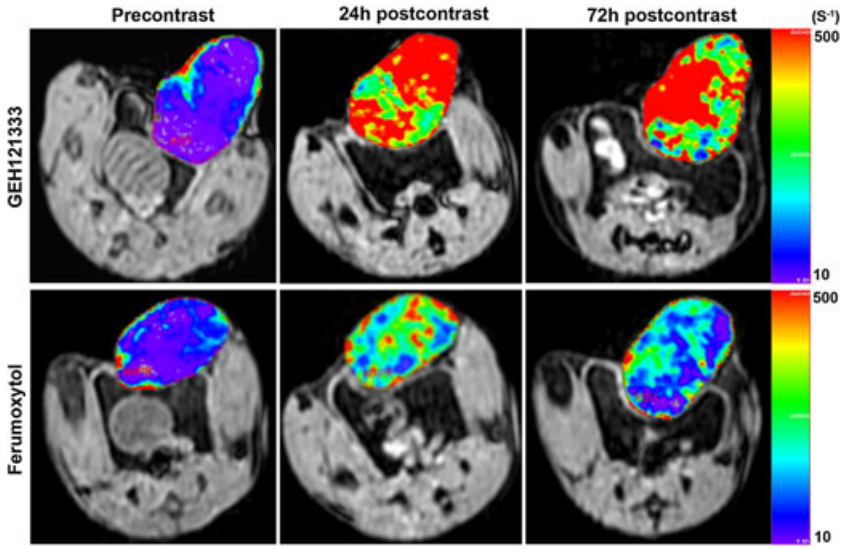

Figure 4. Tumor R_2* maps. Representative tumor R_2* maps before and at 24 and 72 h after injection of GEH121333 and ferumoxytol. The color maps correspond to R_2* values indicated on the scale immediately to their right. On pre-contrast maps, tumors had relatively homogeneous, low R_2* levels. At 24 and 72 h p.i., there was a widespread, inhomogeneous increase in tumor R_2* relaxation rates. GEH121333 produced stronger T_2* enhancement than ferumoxytol.

life and excellent tolerance in rodents and better signal enhancement compared with the iron supplement ferumoxytol.

To date, there is no FDA-approved USPIO contrast agent available for clinical MR imaging applications. Several first-generation USPIOs, such as ferumoxtran-10 (Combidex®/Sinerem®), Supravist™ and feruglose (Clariscan™), have been evaluated in phase II or III clinical trials, but discontinued owing to low efficacy, limited spectrum of applications or safety considerations (19,29–31).

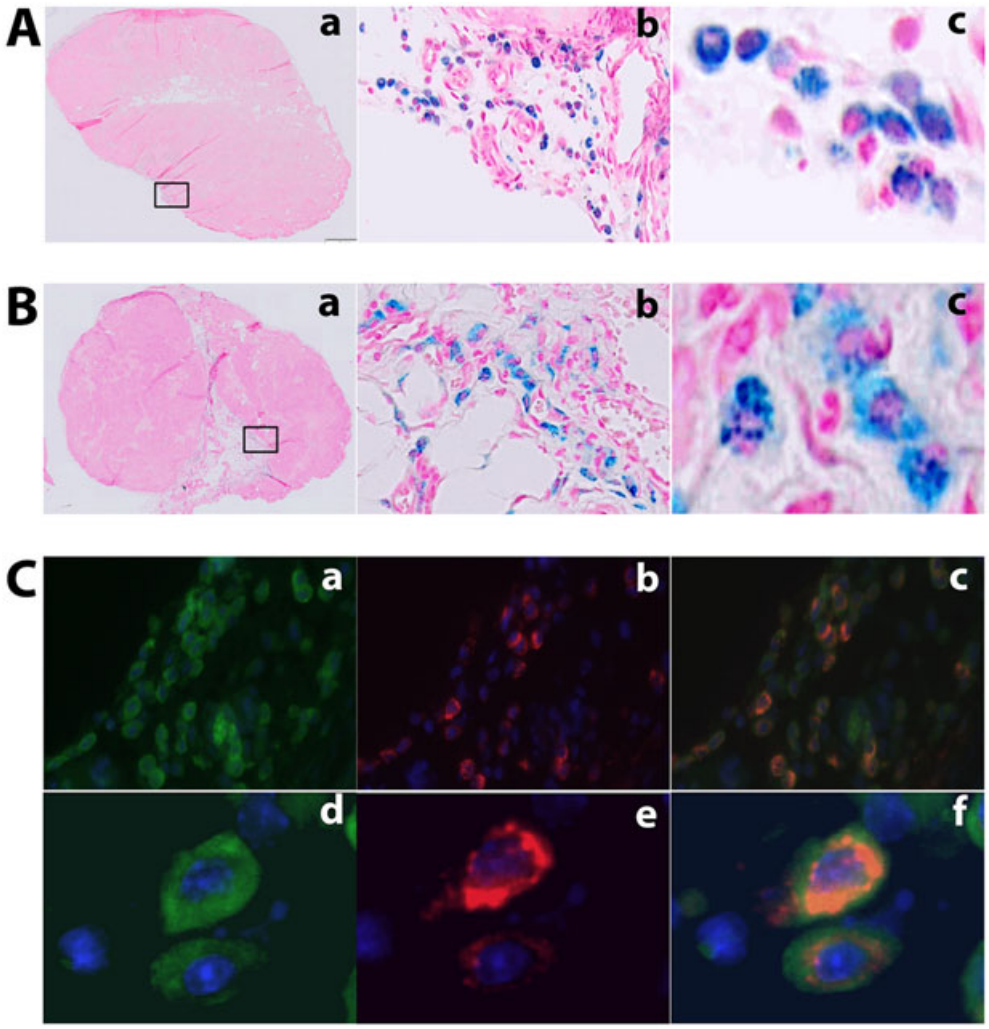

Figure 5. GEH121333 uptake by Tumor-associated macrophages (TAM). (A) Representative Perls stains of GEH121333-treated whole tumors at 72 h post-injection identified iron-reacting cells, mostly in the tumor periphery and around vessels in the tumor center (a, 1×), indicating intracellular iron deposition (b, 20×; c, 60×). (B) Representative Perls stains of ferumoxytol-treated whole tumors at 72 h post-injection also revealed iron-containing cells in tumor tissues (a, 1×; b, 20×; c, 60×). (C) Immunofluorescence assays using anti-PEG-Cy5 (red) and anti-F4/80-Cy3 (green) showed intracellular compartmentalization of GEH121333 nanoparticles (b, 20×; e, 60×) and the presence of TAM in the tumor tissue (a, 20×; d, 60×). Co-localization of TAM and GEH121333 (yellow/orange) confirmed cellular uptake of ultrasmall superparamagnetic iron oxide nanoparticle by TAM (c, 20×; f, 60×) 72 h after intravenous administration.

Second-generation USPIOs provide improved safety profiles and improved T_1-contrast, thereby widening the spectrum of clinical applications. In addition, USPIOs are not associated with a risk of nephrogenic systemic fibrosis and could be used as an alternative to gadolinium-based contrast agents in patients with renal insufficiency (32). Ferumoxytol is a second-generation USPIO that has been FDA-approved as an intravenous iron supplement for anemia treatment in patients with chronic kidney disease (23). Its use in MR imaging remains off-label and investigational (33). This raises several practical issues, as detailed above, that prevent routine use of ferumoxytol for clinical MR imaging.

GEH121333 is a novel second-generation USPIO, being developed as a dedicated MR contrast agent for tumor imaging. GEH121333 shares imaging features with other USPIOs, such as initial blood pool distributuion, slow transendothelial leakage across hyperpermeable tumor microvessels (EPR), and resulting long-lasting tumor enhancement owing to nanoparticle accumulation in the tumor interstitium and TAM phagocytosis. In addition to very good tolerance in rodents, the blood half-life of GEH121333, as estimated in rats by blood relaxometry, is ~2-fold longer than that of ferumoxytol (~4 vs ~2 h, respectively). This implies a slower uptake rate by macrophages in the RES, and possibly also TAM. We attribute this difference to the small size and PEGylation of GEH121333, which lead to slower RES uptake and prolonged half-life (34). To our surprise, GEH121333 produced a stronger T_2* signal loss in tumors than ferumoxytol, even though the former has a lower r_2 relaxivity (40 vs 89 s^{-1} mM^{-1}). This may be explained by the following possible reasons: the prolonged circulation half-life and small and uniform-sized particles with monodisperse configuration of GEH121333 may lead to an increased microvascular permeability (35). The polydispersed ferumoxytol contains larger particles that locate in the tail of the particle size distribution and may show less efficient delivery (36,37). In addition, there could be a more pronounced aggregation of GEH121333 inside the macrophages.

We found GEH121333-containing TAM in patches deep inside the tumor and along vessels in the tumor periphery. This distribution is consistent with prior studies that have demonstrated

attraction of TAM to hypoxic regions in the tumor center (38–40), as well as the vascularized tumor periphery, where they promote angiogenesis, and break down basement membranes and extracellular matrix, supporting vascular tumor cell invasion (38,39,41).

We recognize several limitations of our study. We used a higher (27.92 mg Fe kg^{-1}) than recommended clinical dose for USPIO (5–8 mg Fe kg^{-1}). This increased dose is recommended for USPIO studies in rodents, in order to compensate for the faster iron pharmacokinetics in rodents (19). Future studies have to confirm our observations in a clinical setting.

We noted colorimetric interference with serum chemistry evaluations within 24 h p.i. Of note, interference with colorimetric serum chemistry assays has also been described for gadolinium chelates, although the impact may be due less to the much faster elimination of these agents (42). Further studies are needed to clarify if and for how long interference with colorimetric assays also occurs with clinical GEH121333 applications. Clinicians would have to be educated about alternative noncolorimetric laboratory assays, which could be applied for the time period of potential interference.

As USPIOs are metabolized through endogenous iron salvage pathways, they are generally safe and have low *in vivo* toxicity (43). Likewise, our data showed that GEH121333 was very well tolerated in rodents at high doses of 200 mg Fe kg^{-1}. This is consistent with safety reports of other USPIOs in the same particle size range (10–50 nm) (34,44). However, we did not evaluate the long-term *in vivo* toxicity of GEH121333. Further studies are needed to evaluate the long-term pharmacokinetics of this novel USPIO agent. Our preliminary data suggest faster metabolism of GEH121333 within the RES compared with other USPIOs (unpublished data), which could be advantageous for longitudinal evaluations.

Potential clinical applications: GEH121333 is currently being developed for clinical applications. GEH121333 nanoparticles may serve as an imaging biomarker for TAM infiltration in breast cancers and could be utilized for early therapy stratifications, to inform the development and regulatory approval of novel anti-inflammatory cancer therapies, as well as to monitor response to TAM-targeted therapies. GEH121333 nanoparticle-based TAM detection and quantification may ultimately enable a more individualized cancer treatment, leading to improved prognosis for a large variety of cancers.

4. EXPERIMENTAL

The study was approved by the Institutional Animal Care and Use Committees at the GE Global Research Center and Stanford University. We investigated a novel USPIO contrast agent that was developed and provided by GE Global Research (Niskayuna, NY, USA). Initial tolerance evaluations were performed by investigators from GE Global Research and the associated histopathological analysis of GEH121333-treated animals were carried out by Charles River Laboratories (Frederick, MD, USA). Imaging studies and data analyses were carried out at Stanford University. Histopathologic correlations were obtained by researchers at GE Global Research, who were blinded to the MR imaging data. Only authors who are not employees of or consultants for GE Global Research (R.M., T.D.H., S.B., S.T., S.A., G.P., M.R. and H.E.D.) had control of inclusion of any data and information submitted for publication.

4.1. GEH121333 Contrast Agent

GEH121333 is a new core/shell USPIO agent with an iron oxide core and a hydroxyphosphonate-PEG shell. GEH121333 nanoparticles have an average hydrodynamic diameter of 22 nm, as measured by differential light scattering with near mono-dispersity, as measured by field flow fractionation. GEH121333 nanoparticles have an r_1 relaxivity of 17 s^{-1} mM^{-1} and r_2 relaxivity of 40 s^{-1} mM^{-1} measured at 1.5 T and 40 °C. They undergo rapid processing from RES organs. This feature is particularly appealing when it comes to cancer treatment monitoring, which requires periodic MR imaging.

4.2. Pharmacokinetic Study

GEH121333 was injected through a catheter placed in the lateral tail veins of adult female Fisher rats (Charles River Laboratories, 150–200 g, $n = 4$ each USPIO compound), and was dosed at 5 mg Fe kg^{-1} body weight. The catheter was flushed with 0.9% normal saline following the injection. After 5 min, 300 µl of blood was collected into an ethylene diamine tetraacetic acid (EDTA) blood collection tube via a catheter placed in the contralateral tail vein. Sampling was repeated at 4 h post-injection. The T_1 and T_2 relaxation time constants were determined for the collected blood samples on a Bruker Minispec mq60 (Bruker, Billerica, MA, USA) at 60 MHz and 40 °C. A blood clearance time constant was estimated from the change in relaxation rates ($R_1, 2 = 1/T_1, 2$) over the first 4 h post-injection, after subtracting the corresponding relaxation rate for agent-free whole blood as baseline.

4.3. Tolerance Evaluation

Twelve 6–8 week old Lewis rats (Charles River Laboratories) were randomly divided into three separate cohorts ($n = 4$ per cohort), and received intravenous injections of either 6.7 ml kg^{-1} volume of high dose GEH121333 (200 mg Fe kg^{-1}), hydroxyphosphonate-PEG, or 0.9% saline. Animals were monitored for up to 7 days after injections. Body weights were measured daily and blood was collected before as well as 4 h, 24 h, 48 h and 7 p.i. CBC, including leukocyte, erythrocyte and thrombocyte cell counts were measured with the Hemavet 750FS (Drew Scientific Inc., Waterbury, CT, USA), as per the manufacturer's instructions. Serum chemistry data (albumin, alkaline phosphatase, alanine aminotransferase, amylase, total bilirubin, blood urea nitrogen, creatinine, calcium, phosphorus, glucose, sodium, potassium, total protein and globulins) were obtained by an Abaxis VetScan VS2 with the Comprehensive Diagnostic Profile reagent rotor (Abaxis Inc., Union City, CA, USA), following the manufacturer's instructions. At 7 days post-injection, animals were euthanized by CO_2, gross necropsy was performed and the following tissues were collected in 10% formalin for histopathological analysis: spleen, liver, kidneys, heart, lungs and bone (tibia). Tissues were sent to Charles River Laboratories for further processing, along with hematoxylin–eosin staining and evaluation by licensed veterinarian pathologists.

4.4. MR Imaging

Breast adenocarcinoma cells isolated from 90–95 day old transgenic MMTV-PyMT mice were implanted into the left lower mammary fat pad of 23 postpubertal, 10–12 week-old female FVB/n mice to generate breast cancer mouse models as previously described (45). When tumors reached a size of 1.5 cm, animals underwent MR imaging under isofluorane anesthesia, using a 7 T animal MR scanner (General Electric-Varian microSigna 7.0)

and a dedicated single-channel transmit/receive birdcage radiofrequency coil (inner diameter of 2 cm). Animals were randomly divided into three experimental groups that received intravenous administrations of GEH121333 ($n = 10$) or ferumoxytol ($n = 9$) at 27.92 mg Fe kg^{-1} body weight (= 0.5 mmol Fe kg^{-1}) or were left untreated ($n = 4$). Ferumoxytol (Feraheme®, AMAG Pharmaceuticals Inc., Cambridge, MA, USA) consisted of multidisperse nanoparticles with a Fe_3O_4 core and a carbohydrate coating. The nanoparticles had a mean hydrodynamic diameter of 30 nm, an r_1 relaxivity of 15 s^{-1} mM^{-1} and r_2 relaxivity of 89 s^{-1} mM^{-1} (1.5 T, 37 °C) (19). MR images were obtained before USPIO injection and at 1, 24, 48 and 72 h p.i., using the following pulse sequences: T_1-weighted three-dimensional fast spoiled gradient recalled acquisition 6.6 ms/1.4 ms/2–30°/112 × 112 pixels (repetition time/echo time/flip angle/matrix) and fast gradient echo 6.6 ms/1.4 ms/15°/112 × 112 pixels, T_2-weighted three-dimensional fast gradient echo 70 ms/1.6–20.5 ms (10 echoes with echo spacing of 2.1 ms)/20°/128 × 96pixels and 2D fast spin echo 4000 ms/42 ms/90°/128 × 128pixels (echo train length of 8). All MR acquisitions were performed with a field of view of 4.5 cm and a slice thickness of 0.6 mm.

MR data were analyzed by one independent investigator at Stanford (Q.S.) using custom research software tool (Cinetool, GE Global Research Center). T_1 and T_2* relaxation times of tumors were calculated based on multi-flip-angle fast spoiled gradient recalled and multi-echo fast gradient echo images, converted to relaxation rates ($R_1 = 1/T_1$, $R_2^* = 1/T_2^*$) and displayed as relaxometric maps. Changes in relaxation rates (ΔR_1 and ΔR_2^*) after iron oxide administration were calculated by subtracting pre-contrast from post-contrast relaxation rates.

4.5. Tumor Histopathology

GEH121333 and ferumoxytol-treated animals were sacrificed for histological correlation at 24 h ($n = 2$ each), 48 h ($n = 2$ each) and 72 h ($n = 6$ GEH121333, $n = 5$ ferumoxytol) p.i. Four additional tumor-bearing mice served as untreated controls. Mammary tumors were explanted, fixed in 10% formalin, dehydrated and embedded in paraffin for histological processing. Formalin-fixed paraffin embedded whole tumor tissue sections were deparaffinized with Histochoice clearing agent (Amresco, Solon, OH, USA), rehydrated by a series of alcohol washes, and processed for iron stains and antigen retrieval. Perls iron stains of whole tumor tissue sections were performed using the Iron Stain Kit (American MasterTech, Lodi, CA, USA) following the manufacturer's instructions and counter-stained with nuclear fast red.

Immunofluorescence detection of TAM and GEH121333 in tumor tissue was performed using an antigen retrieval method. In brief, slides were washed in phosphate buffered saline (PBS) with citrate buffer for 20 min followed by 0.3% Triton X-100/EDTA for 20 min and blocked against nonspecific binding by incubating with blocking solution (10% goat serum/PBS) for 1–2 h at room temperature. A mixture of two primary antibodies containing (1) anti-PEG, rabbit-derived (Epitomics Inc., Burlingame, CA, USA) and (2) rat anti-mouse F4/80 (Serotec, Oxford, UK) was applied on the sections at a dilution of 1:100 and left overnight at 4 °C in PBS/10% goat serum. For indirect detection of bound primary antibodies, species-specific Cy3 or Cy5-conjugated secondary antibodies were used at a dilution of 1:200. The sections were further stained with 4′,6-diamidino-2-phenylindole (DAPI) to identify cell nuclei.

A pathologist who was blinded to the MR data determined whether stains were positive for iron, GEH121333, and TAM in tumor tissues, using a Zeiss Mirax Scan Microscope (Zeiss, Oberkochen, Germany) and a Zeiss fluorescence microscope with DAPI, Cy3 and Cy5 channels.

4.6. Statistical Analysis

Data are presented as mean ± standard deviation (SD) unless otherwise specified. Quantitative MR data of tumors were compared between different contrast agent groups and different time points before and after iron oxide administration, using a linear mixed effects model with a random effect for each animal. Results were considered statistically significant when $p < 0.05$.

5. CONCLUSIONS

MR imaging with GEH121333 nanoparticles represents a novel biomarker for TAM assessment. This new, well-tolerated USPIO MR contrast agent provides a longer blood half-life and better TAM enhancement compared with the iron supplement ferumoxytol.

Supporting Information

Supporting information can be found in the online version of this article.

Acknowledgments

We thank the GE Global Research chemistry team for their efforts in developing and supplying the GEH121333 agent, and Sandeep Gupta for providing the Cinetool software for MR data analyses. This work was in part supported by a grant from the National Cancer Institute (NIH/NCI; grant number R21CA156124), a Developmental Cancer Research Award from the Stanford Cancer Institute, and a Pilot Grant from GE Healthcare.

REFERENCES

1. Kawamura K, Komohara Y, Takaishi K, Katabuchi H, Takeya M. Detection of M2 macrophages and colony-stimulating factor 1 expression in serous and mucinous ovarian epithelial tumors. Pathol Int 2009; 59(5): 300–305.
2. Mroczko B, Groblewska M, Wereszczynska-Siemiatkowska U, Okulczyk B, Kedra B, Laszewicz W, Dabrowski A, Szmitkowski M. Serum macrophage-colony stimulating factor levels in colorectal cancer patients correlate with lymph node metastasis and poor prognosis. Clinica Chim Acta 2007; 380(1–2): 208–212.
3. Sica A, Schioppa T, Mantovani A, Allavena P. Tumour-associated macrophages are a distinct M2 polarised population promoting tumour progression: potential targets of anti-cancer therapy. Eur J Cancer 2006; 42(6): 717–727.
4. Zhu XD, Zhang JB, Zhuang PY, Zhu HG, Zhang W, Xiong YQ, Wu WZ, Wang L, Tang ZY, Sun HC. High expression of macrophage colony-stimulating factor in peritumoral liver tissue is associated with poor survival after curative resection of hepatocellular carcinoma. J Clin Oncol 2008; 26(16): 2707–2716.
5. Heusinkveld M, van der Burg SH. Identification and manipulation of tumor associated macrophages in human cancers. J Translat Med 2011; 9: 216.
6. Osinsky S, Bubnovskaya L, Ganusevich I, Kovelskaya A, Gumenyuk L, Olijnichenko G, Merentsev S. Hypoxia, tumour-associated macrophages, microvessel density, VEGF and matrix metalloproteinases in human gastric cancer: interaction and impact on survival. Clin Transl Oncol 2011; 13(2): 133–138.
7. Toge H, Inagaki T, Kojimoto Y, Shinka T, Hara I. Angiogenesis in renal cell carcinoma: the role of tumor-associated macrophages. Int J Urol 2009; 16(10): 801–807.

8. Ruffell B, Affara NI, Coussens LM. Differential macrophage programming in the tumor microenvironment. Trends Immunol 2012; 64(2): 179–189.
9. Kuang DM, Zhao Q, Peng C, Xu J, Zhang JP, Wu C, Zheng L. Activated monocytes in peritumoral stroma of hepatocellular carcinoma foster immune privilege and disease progression through PD-L1. J Exp Med 2009; 206(6): 1327–1337.
10. Mizutani K, Sud S, McGregor NA, Martinovski G, Rice BT, Craig MJ, Varsos ZS, Roca H, Pienta KJ. The chemokine CCL2 increases prostate tumor growth and bone metastasis through macrophage and osteoclast recruitment. Neoplasia 2009; 11(11): 1235–1242.
11. Tanaka K, Kurebayashi J, Sohda M, Nomura T, Prabhakar U, Yan L, Sonoo H. The expression of monocyte chemotactic protein-1 in papillary thyroid carcinoma is correlated with lymph node metastasis and tumor recurrence. Thyroid 2009; 19(1): 21–25.
12. Bingle L, Brown NJ, Lewis CE. The role of tumour-associated macrophages in tumour progression: implications for new anticancer therapies. J Pathol 2002; 196(3): 254–265.
13. Ryder M, Ghossein RA, Ricarte-Filho JC, Knauf JA, Fagin JA. Increased density of tumor-associated macrophages is associated with decreased survival in advanced thyroid cancer. Endocrine-relat Cancer 2008; 15(4): 1069–1074.
14. Niino D, Komohara Y, Murayama T, Aoki R, Kimura Y, Hashikawa K, Kiyasu J, Takeuchi M, Suefuji N, Sugita Y, Takeya M, Ohshima K. Ratio of M2 macrophage expression is closely associated with poor prognosis for angioimmunoblastic T-cell lymphoma (AITL). Pathol Int 2010; 60 (4): 278–283.
15. Allavena P, Signorelli M, Chieppa M, Erba E, Bianchi G, Marchesi F, Olimpio CO, Bonardi C, Garbi A, Lissoni A, de Braud F, Jimeno J, D'Incalci M. Anti-inflammatory properties of the novel antitumor agent yondelis (trabectedin): inhibition of macrophage differentiation and cytokine production. Cancer Res 2005; 65(7): 2964–2971.
16. Dewar AL, Cambareri AC, Zannettino AC, Miller BL, Doherty KV, Hughes TP, Lyons AB. Macrophage colony-stimulating factor receptor c-fms is a novel target of imatinib. Blood 2005; 105(8): 3127–3132.
17. Hiraga T, Nakamura H. Imatinib mesylate suppresses bone metastases of breast cancer by inhibiting osteoclasts through the blockade of c-Fms signals. Int J Cancer 2009; 124(1): 215–222.
18. Daldrup-Link HE, Golovko D, Ruffell B, Denardo DG, Castaneda R, Ansari C, Rao J, Tikhomirov GA, Wendland MF, Corot C, Coussens LM. MRI of tumor-associated macrophages with clinically applicable iron oxide nanoparticles. Clin Cancer Res 2011; 17(17): 5695–5704.
19. Corot C, Robert P, Idee JM, Port M. Recent advances in iron oxide nanocrystal technology for medical imaging. Adv Drug Deliv Rev 2006; 58(14): 1471–1504.
20. Shih YY, Hsu YH, Duong TQ, Lin SS, Chow KP, Chang C. Longitudinal study of tumor-associated macrophages during tumor expansion using MRI. NMR Biomed 2011; 24(10): 1353–1360.
21. Weissleder R, Elizondo G, Wittenberg J, Lee AS, Josephson L, Brady TJ. Ultrasmall superparamagnetic iron oxide: an intravenous contrast agent for assessing lymph nodes with MR imaging. Radiology 1990; 175(2): 494–498.
22. Kowalczyk M, Banach M, Rysz J. Ferumoxytol: a new era of iron deficiency anemia treatment for patients with chronic kidney disease. J Nephrol 2011; 24(6): 717–722.
23. Lu M, Cohen MH, Rieves D, Pazdur R. FDA report: Ferumoxytol for intravenous iron therapy in adult patients with chronic kidney disease. Am J Hematol 2010; 85(5): 315–319.
24. Landry R, Jacobs PM, Davis R, Shenouda M, Bolton WK. Pharmacokinetic study of ferumoxytol: a new iron replacement therapy in normal subjects and hemodialysis patients. Am J Nephrol 2005; 25(4): 400–410.
25. Singh A, Patel T, Hertel J, Bernardo M, Kausz A, Brenner L. Safety of ferumoxytol in patients with anemia and CKD. Am J Kidney Dis 2008; 52(5): 907–915.
26. Ho DH, Brown NS, Yen A, Holmes R, Keating M, Abuchowski A, Newman RA, Krakoff IH. Clinical pharmacology of polyethylene glycol-L-asparaginase. Drug Metab Dispos 1986; 14(3): 349–352.
27. Gabizon AA. Pegylated liposomal doxorubicin: metamorphosis of an old drug into a new form of chemotherapy. Cancer Invest 2001; 19(4): 424–436.
28. Knop K, Hoogenboom R, Fischer D, Schubert US. Poly(ethylene glycol) in drug delivery: pros and cons as well as potential alternatives. Angew Chem (Int Edn) 2010; 49(36): 6288–6308.
29. Thorek DL, Chen AK, Czupryna J, Tsourkas A. Superparamagnetic iron oxide nanoparticle probes for molecular imaging. Ann Biomed Eng 2006; 34(1): 23–38.
30. Daldrup-Link HE, Rydland J, Helbich TH, Bjornerud A, Turetschek K, Kvistad KA, Kaindl E, Link TM, Staudacher K, Shames D, Brasch RC, Haraldseth O, Rummeny EJ. Quantification of breast tumor microvascular permeability with feruglose-enhanced MR imaging initial phase II multicenter trial. Radiology 2003; 229(3): 885–892.
31. Barentsz JO, Futterer JJ, Takahashi S. Use of ultrasmall superparamagnetic iron oxide in lymph node MR imaging in prostate cancer patients. Eur J Radiol 2007; 63(3): 369–372.
32. Neuwelt EA, Hamilton BE, Varallyay CG, Rooney WR, Edelman RD, Jacobs PM, Watnick SG. Ultrasmall superparamagnetic iron oxides (USPIOs): a future alternative magnetic resonance (MR) contrast agent for patients at risk for nephrogenic systemic fibrosis (NSF)? Kidney Int 2009; 75(5): 465–474.
33. Hamilton BE, Nesbit GM, Dosa E, Gahramanov S, Rooney B, Nesbit EG, Raines J, Neuwelt EA. Comparative analysis of ferumoxytol and gadoteridol enhancement using T1- and T2-weighted MRI in neuroimaging. AJR Am J Roentgenol 2011; 197(4): 981–988.
34. Dufort S, Sancey L, Coll JL. Physico-chemical parameters that govern nanoparticles fate also dictate rules for their molecular evolution. Adv Drug Deliv Rev 2012; 33(3):119–126.
35. Tang L, Fan TM, Borst LB, Cheng J. Synthesis and biological response of size-specific, monodisperse drug-silica nanoconjugates. ACS Nano 2012; 6(5): 3954–3966.
36. Castaneda RT, Khurana A, Khan R, Daldrup-Link HE. Labeling stem cells with ferumoxytol, an FDA-approved iron oxide nanoparticle. J Vis Exp 2011; 57: e3482.
37. Xu Q, Hashimoto M, Dang TT, Hoare T, Kohane DS, Whitesides GM, Langer R, Anderson DG. Preparation of monodisperse biodegradable polymer microparticles using a microfluidic flow-focusing device for controlled drug delivery. Small 2009; 5(13): 1575–1581.
38. Mantovani A, Marchesi F, Porta C, Sica A, Allavena P. Inflammation and cancer: breast cancer as a prototype. Breast 2007; 16(suppl 2): S27–33.
39. Ahmed F, Wyckoff J, Lin EY, Wang W, Wang Y, Hennighausen L, Miyazaki J, Jones J, Pollard JW, Condeelis JS, Segall JE. GFP expression in the mammary gland for imaging of mammary tumor cells in transgenic mice. Cancer Res 2002; 62(24): 7166–7169.
40. Leek RD, Talks KL, Pezzella F, Turley H, Campo L, Brown NS, Bicknell R, Taylor M, Gatter KC, Harris AL. Relation of hypoxia-inducible factor-2 alpha (HIF-2 alpha) expression in tumor-infiltrative macrophages to tumor angiogenesis and the oxidative thymidine phosphorylase pathway in Human breast cancer. Cancer Res 2002; 62(5): 1326–1329.
41. Hildenbrand R, Dilger I, Horlin A, Stutte HJ. Urokinase and macrophages in tumour angiogenesis. Br J Cancer 1995; 72(4): 818–823.
42. Normann PT, Froysa A, Svaland M. Interference of gadodiamide injection (OMNISCAN) on the colorimetric determination of serum calcium. Scand J Clin Lab Invest 1995; 55(5): 421–426.
43. Rosenblum LT, Kosaka N, Mitsunaga M, Choyke PL, Kobayashi H. In vivo molecular imaging using nanomaterials: general in vivo characteristics of nano-sized reagents and applications for cancer diagnosis. Mol Membr Biol 2010; 27(7): 274–285.
44. Elizondo G, Weissleder R, Stark DD, Guerra J, Garza J, Fretz CJ, Todd LE, Ferrucci JT. Hepatic cirrhosis and hepatitis: MR imaging enhanced with superparamagnetic iron oxide. Radiology 1990; 174(3 Pt 1): 797–801.
45. Guy CT, Cardiff RD, Muller WJ. Induction of mammary tumors by expression of polyomavirus middle T oncogene: a transgenic mouse model for metastatic disease. Mol Cell Biol 1992; 12(3): 954–961.